AIAA Journal

VOLUME 3 SEPTEMBER 1965 NUMBER 9

Geomagnetically Trapped Radiation

M. B. Baker
Douglas Aircraft Co., Inc., Santa Monica, Calif.

1. Introduction

THE magnetic field of the earth is similar to that of a dipole and can contain large numbers of trapped charged particles in its magnetic bottlelike configuration. This had been recognized for some time (see, e.g., Singer)[1] before the discovery was made in 1958 by Explorers I and III[2] of naturally occurring trapped particles, subsequently called Van Allen radiation. Since then, additions to the natural population of the trapped particle region have been made in the form of energetic electrons released by high-altitude nuclear bursts.[3,4]

A major objective of this report is to provide a comprehensive description of the trapped charged-particle environment that can be used to find the radiation doses to which a vehicle will be exposed. The second and third sections contain a description of the trapped radiation environment, including a discussion of the sources and loss mechanisms and the dynamics of the particle motions, a description of the sources of the data and the compilation techniques, and graphic displays of the fluxes. The fourth section presents the fluxes and energy spectra integrated over sample trajectories.

2. Dynamics of Particle Motion

2.1 Motions of the Particles

The motions of the trapped charged particles in the geomagnetic field are well understood for the unperturbed situation. Detailed descriptions of the dynamics of charged particle motion have been given by many authors, including Alfvén,[5] Northrop and Teller,[6] and Northrop.[7] The latter reference was the source of information for much of the following discussion.

The force $\mathbf{F}$ on a particle having a charge q moving with a velocity $\mathbf{v}$ in a magnetic field $\mathbf{B}$ and electric field $\mathbf{E}$ is the well-known Lorentz force

$$\mathbf{F} = q(\mathbf{E} + \mathbf{v} \times \mathbf{B}) \quad (1)$$

If the magnetic field is uniform and time-independent and there is no electric field, the motion will be helical around a line of force. This can alternatively be described as motion about a circle whose center is moving along the line of force. The center of this circle is called the "guiding center," and its radius is the Larmor radius ρ of the particle.

If the field differs slightly from uniformity and time-independence, or if there exists an electric field, the path of the particle will be different from a helix. However, it will be similar to a helix, and the particle therefore can be described as moving about a circle whose center now has a component of velocity at right angles to the field line.

The transverse motion is called the "drift" and is made up of eight components. The three most well-known are the $\mathbf{E} \times \mathbf{B}$ drift, the gradient $\mathbf{B}$ drift, and the line curvature drift. The first is seen in the presence of an external electric field. The second is caused by the radius of curvature of the path being smaller on one side of the "circle" of gyration, where the field is stronger, than on the other. The third is caused by the centripetal force produced by the curved path of the guiding center along the curved field lines.

The other sources of drift are perhaps less familiar and less geometrically obvious, but in certain situations they can be important. One is proportional to the change of $\mathbf{B}$ with time and is due to a change in the relative magnitudes of the particle velocity perpendicular to and parallel to $\mathbf{B}$ as $\mathbf{B}$ changes in direction during one Larmor period. The other four of the eight drift terms contain $\mathbf{E} \times \mathbf{B}$ again, and in many cases this is negligibly small. However, the $(\mathbf{E} \times \mathbf{B}) - \nabla(\mathbf{E} \times \mathbf{B})$ term is responsible for the shear (or Helmholtz) instability of a plasma which occurs, for instance, at the interface between the solar wind and the geomagnetic field.

The field lines in the geomagnetic field converge toward the earth's surface. A charged particle spiraling along a field line will therefore see a component of the field directed in toward its guiding center. This will exert a Lorentz force on the particle in the direction opposite to the convergence of the field. The particle will experience this force as a retarding

M. B. Baker is a physicist in the Space Sciences Department, Missile and Space Systems Division at the Douglas Aircraft Co. He has been engaged in studies of the space radiation environment since 1961 when he left the University of Florida with an M.S. in Physics. He was a National Science Foundation Cooperative Graduate Fellow and did his thesis research in astronomical physics. Recently, he has been working in the fields of solar cosmic radiation and cosmology, in addition to the morphology of trapped charged particles.

Received November 20, 1964; revision received May 18, 1965. Work presented herein was conducted by the Douglas Missile and Space Systems Division under company-sponsored Research and Development funds. It is a pleasure to acknowledge valuable programing assistance from L. E. Krichesky.

force as it moves downward, away from the equator, until it reverses its direction and returns toward the equator and down the other side. In other words, if α is the pitch angle of the particle, the angle between **v** and **B**, then α increases from α_0 at the magnetic equator to 90° at the point at which it reverses direction. The point at which the particle reverses its direction is called the mirror point, and it is this mirroring phenomenon that traps the particles.

2.2 Adiabatic Invariants

The particles can be considered to have three different superimposed motions: spiraling around the field lines, oscillating back and forth along the field lines between their mirror points, and drifting across the field lines. The constraint of the particles to certain regions of space which are usually called the trapping regions can be described in terms of three so-called adiabatic invariants. They are quantities that remain approximately constant when perturbations are applied slowly compared to the characteristic periods of the motions of the particles. The first adiabatic invariant is the magnetic moment. If the particle in its path around the field line is treated as a current loop, its magnetic moment can be shown to be

$$\mu = \tfrac{1}{2}(1 - \beta^2)^{-1/2} mv^2 (\sin^2\alpha/B) \tag{2}$$

where $\beta = v/c$.

Alfvén[5] has shown that μ is constant when

$$|\text{grad}B/B| \ll 1/\rho \tag{3}$$

$$|\partial B/\partial t| \ll B\nu \tag{4}$$

where ρ is the Larmor radius and ν the Larmor frequency of the particle. Furthermore, in the unperturbed situation, the kinetic energy of the particle is constant, so the term $\sin^2\alpha/B$ is also constant. This allows the value of B at the mirror point (B_m) of the particle to be determined if α_0 is known, since $\alpha = 90°$ there. It can be shown that, since the magnetic field gets weaker as the altitude increases, a point will eventually be reached where the variation of B over the radius of gyration of the particle is not negligible, so Eq. (3) will not be satisfied, and the invariance of μ will break down at higher altitudes.

The second or longitudinal invariant is

$$I = \int (1 - B/B_m)^{1/2} ds \tag{5}$$

integrated along the guiding center path between the mirror points. Whereas the first adiabatic invariant restricts the particles to paths that mirror at a constant geomagnetic field intensity (B_m), the second adiabatic invariant restricts the drift of the particle to field lines on which I is a constant. Again, I is constant only for slow perturbations; in this case the time variations of the field must be small compared to the "bounce period," the time it takes a particle to complete an oscillation from one mirror point to the opposite one and back. Since a particle makes many gyrations around a field line in each bounce period, the second adiabatic invariant is more easily invalidated than the first in a time-dependent field. When this occurs, particles may move to lower field lines and be lost in the atmosphere.

The third adiabatic invariant is the total flux of B inside the surface formed by the particle as it drifts in longitude. The flux invariant guarantees that this surface will be closed. In a manner analogous to the other two invariants, the flux is invariant only when the field remains nearly constant for the time it takes the particles to drift in longitude around the earth, i.e., the drift period.

These adiabatic invariants can be used to predict the behavior of trapped particles. However, they are subject to the stringent requirements described previously. The circumstances under which the invariance of any of these quantities breaks down are not known quantitatively. For instance, the breakdown of the first invariant at high altitudes, as previously described, has not been demonstrated to be dominant in any region.

2.3 Magnetic Coordinates

Since a trapped particle is confined to a shell of magnetic field lines having a constant I and B_m, these two parameters can be used as coordinates for mapping the fluxes of particles. The number of coordinates necessary is reduced from three to two. McIlwain,[8] however, reasoned that a parameter that retained the geomagnetic significance of I and in addition was approximately constant on a given line of force would be even more useful. In a dipole field, such a parameter is R_0, the radial distance to the point where the field line crosses the equatorial plane. Radiation trapped in a dipole field can be completely specified in terms of R_0 and B, where R_0 specifies a field shell, and B specifies a pair of positions on that field shell. Since in a dipole field the particles are constrained to field lines having the same R_0 and oscillate in such a manner that the pitch angle of each particle is the same at the same value of B as a consequence of Eq. (2), the flux at a point in space having the magnetic coordinates (B, R_0) is the same as the flux at every other point having the same magnetic coordinates.

The real geomagnetic field, however, differs from a dipole field. Therefore, McIlwain devised the magnetic field parameter L, which has the same function in the real field that R_0 has in the dipole field. The real field is in practice approximated by a multiterm expansion, such as that of Jensen and Cain.[9] This expansion is used by McIlwain's computer subprogram INVAR to calculate B and I and, in turn, L. In general, L is found to vary less than about 1% along a field line.

It must be remembered that the B, L coordinate system is based on the assumption of the conservation of the adiabatic invariants, which is certainly not valid during large geomagnetic storms or at high latitudes and altitudes where the field lines are distorted by the solar wind. However, the concept is generally quite useful and has brought a large measure of consistency to a welter of apparently unrelated measurements.

One disadvantage of B, L coordinates is that they are not intuitively meaningful. This can be somewhat overcome by a reverse transformation to R, λ coordinates using the dipole relations

$$B = M/R^3(4 - 3R/L)^{1/2} \qquad R = L\cos^2\lambda \tag{6}$$

where M is the dipole moment of the earth. In a system in which the real field is transformed into a dipole field, R and λ are in effect the radial distance and latitude. Particle flux maps in this coordinate system are similar to cuts through the real trapping region at a constant longitude in the manner of the picture presented by Van Allen and Frank.[10] Although variations in the geomagnetic field are eliminated by this transformation, the real geographic coordinates are distorted; R at the surface of the earth varies by about ±7%.

2.4 Sources and Loss Mechanisms

In the foregoing discussion, little mention has been made of the mechanisms by which particles are lost from the belts, and no mention has been made of the sources of the particles. The reason for these omissions is that little is known about the relative importance of various possible sources and loss mechanisms.

The only source that has been quantitatively evaluated to any extent is albedo neutrons (see, e.g., Kellogg,[11] Singer,[12] Lencheck and Singer[13]). These are the neutrons produced by nuclear interactions caused by cosmic rays striking the atoms in the atmosphere. A significant fraction of the neu-

trons travel upward, and some of these decay into a proton and an electron before leaving the magnetosphere. If the proton or electron is produced in a region where the magnetic field is strong enough to trap the particle, and if furthermore its pitch angle is large enough so that it can be trapped, it will become trapped.

Calculations of the fluxes and energy spectra of protons and electrons thus trapped have been made.[14] When these calculations are compared to the experimental data, it is apparent that the albedo neutrons are certainly an important source of trapped particles, but not the sole source. The distribution and energy spectra of high-energy protons and perhaps of all of the electrons having energies of several hundred kev in the "inner" zone can be accounted for by albedo neutrons. However, the high fluxes of low-energy protons and electrons found throughout the trapping region and most of the electrons in the "outer" zone apparently cannot be explained by this source.

These calculations and others have in general assumed that the dominant loss mechanism has been interactions with the residual atmosphere. This is the obvious mechanism, and most likely the correct one in large parts of the trapping region. However, other loss mechanisms, such as the breakdown of the first adiabatic invariant previously discussed and scattering of the particles into the loss cone by hydromagnetic waves, probably occur and may be predominant in other parts of the trapping region. Also, at least one other source of trapped particles apparently must exist. The most likely sources are the large continual flux in the solar wind and the sporadic solar cosmic-ray events. There are major obstacles to overcome in explaining how these particles can be injected into trapped orbits within the geomagnetic field, and quantitative theories are presently nonexistent. Solar particles would probably have to be accelerated in order to explain the observed energy spectra even if they did get into the geomagnetic field. The mechanisms now being examined include hydromagnetic waves, the "betatron" acceleration produced when the geomagnetic field varies during magnetic storms, and a combination of acceleration and injection in the shock front just outside the magnetosphere where the geomagnetic field is interacting with the solar plasma. A discussion of many of these ideas and others can be found in O'Brien.[15]

3. Description of the Radiation Environment

3.1 Experimental Requirements

The object of measurements in the trapped radiation zone is to determine the characteristics of the trapped particles. One set of parameters that determines these characteristics is as follows:

j_i = unidirectional intensity of particles of type i having energies between E and $E + dE$
r, λ, θ = geographic coordinates of a point in space
l, m, n = direction cosines of the direction in space being considered
E = particles' kinetic energy
t = time

However, the radiation of any point is approximately symmetrical around a field line, so all particle directions with a pitch angle α are equivalent. Also, a particular magnetic shell is uniquely described by one value of the geomagnetic parameter L. Furthermore, the subsequent position and pitch angle of a particle on a particular L shell is determined by the pitch angle α_0 at the position of minimum $B(B_0)$, at the magnetic equator. Thus the measurement of

$$j_i = j_i(L, \alpha_0, E) \tag{7}$$

for all L, α_0, and E at one time would give a complete and accurate description of the trapped particle fluxes and energy spectra at that instant of time. This could be done in principle with a detector that measures the fluxes of all types of particles vs energy and direction as the detector moves radially outward on the magnetic equator.

An alternate method involves the omnidirectional flux J_i, where

$$J_i = \int_0^{2\pi} \int_0^{\pi} j_i \sin\alpha \, d\alpha \, d\phi \tag{8}$$

The omnidirectional flux is not a function of direction, so it must be measured at each different nonequivalent position in space, i.e., at each value of B on each L shell,

$$J_i = J_i(L, B, E) \tag{9}$$

Therefore, a vehicle carrying omnidirectional detectors for the various particles and energies must cover all L and B positions.

It is frequently desirable to change from one of these systems to the other. Consider the problem of converting a measurement of j_i (L, α_0, E) to an omnidirectional flux J_i (L, B, E). From Eq. (2), invoking the constancy of μ and the particle's kinetic energy we have

$$\sin^2\alpha/B = \sin^2\alpha_0/B_0 \tag{10}$$

If we assume that the flux is azimuthally symmetric, and let $\cos\alpha = u'$ and $\cos\alpha_0 = u$, then

$$j_i\,(L, B, E) = 4\pi \int_0^1 j_i\,(L, u', E)\, du' \tag{11}$$

Also, differentiating Eq. (10)

$$du'/du = (u/u')(B/B_0) \tag{12}$$

Furthermore, since $u' = \cos\alpha = (1 - \sin^2\alpha)^{1/2}$, and $u^2 = \cos^2\alpha_0 = 1 - \sin^2\alpha_0$, and since from Eq. (10) $\sin^2\alpha = (B/B_0)\sin^2\alpha_0$, then

$$u' = [1 - (B/B_0)(1 - u^2)]^{1/2} \tag{13}$$

Finally, inserting Eqs. (12) and (13) into Eq. (11), we get

$$J_i\,(L, B, E) = 4\pi \frac{B}{B_0} \int_{u_1}^1 j_i\,(L, u, E) \times \left[1 - \frac{B}{B_0}(1 - u^2)\right]^{-1/2} u \, du \tag{14}$$

where

$$u_1 = [1 - (B/B_0)^{1/2}]$$

Equation (14) gives the omnidirectional flux at any point along a field line as a function of the unidirectional flux at the magnetic equator.

To date no experiment has satisfied either set of requirements. The earliest satellites carried only simple omnidirectional counters, which counted only the fluxes of particles having energies greater than some rather poorly defined minimum over a limited region of space and were unable in general to distinguish between the various particles. Interpretation of these measurements led to estimates of particle fluxes which were as much as three orders of magnitude in error. One of the better of these early experiments was a pair of shielded G-M counters on Explorer IV. This satellite covered an extensive region of B, L space, and the counters, which were assumed to be counting protons at L values of less than about 2, produced reasonably accurate relative flux data for the two different minimum energies.[16] These data were the basis for the proton energy spectrum published by McIlwain and Pizzella[17] and used in this paper. Even for this experiment, however, it has not been definitely demonstrated that the counters were not, in fact, seeing some electrons.

Probably the most definitive of the later experiments has been McIlwain's[18] on Explorer XV. This satellite again covered an extensive region of B, L space, and its almost

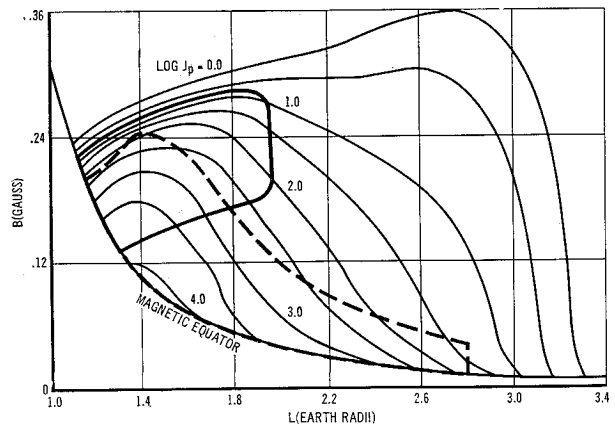

Fig. 1 Omnidirectional proton flux J_p ($40 < E < 100$ Mev) in B, L coordinates.

omnidirectional scintillation counters unambiguously detected protons with energies between 40 and 110 Mev, electrons with energies greater than 0.5 Mev, and electrons with energies greater than 5 Mev. Although the spectral information generated was small, it did give fluxes of both protons and electrons independently.

3.2 Protons

The most accurate and recent trapped proton data available for this study were from Explorer XV by McIlwain[18] and Air Force polar orbiting satellites 1962 AT1 and 1962 BE1 by Freden and Paulikas.[19] The fluxes at other positions were obtained by normalizing other data to these and taking into account the distribution changes with time since the measurements were made, as explained later. The most useful data for this were from Explorer IV,[20, 17, 8] Explorer VII,[20] rocket experiments,[21] other Air Force satellites,[22] and Sputniks II and III.[23,24]

The simplest available analytical expression for the proton energy spectrum which takes into account the softening of the spectrum with increasing L is due to McIlwain and Pizzela.[17] This spectrum is

$$J_p(E)\,dE = Ke^{-E/E_0}dE \tag{15}$$

where

$$E_0 = (306 \pm 28)\,L^{-(5.2\pm0.2)}\ \text{Mev}$$

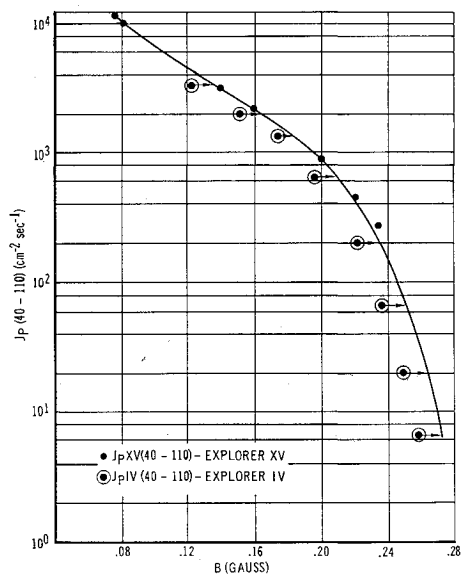

Fig. 2 Omnidirectional proton flux at $L = 1.6$ ($40 < E < 100$ Mev).

Later data[25] indicate that this variation is too simple; the spectrum appears to harden slightly for $L > 1.9$. This will cause thick-shield doses for high-altitude oribits to be too low.

The method used to determine the proton flux distribution shown in Fig. 1 is as follows:

1) The flux of protons with energies between 40 and 110 Mev from Explorer XV, $J_{p\text{XV}}$ (40–110), was plotted vs B at constant L.

2) The flux of protons with energies greater than 31 Mev from Explorer IV, $J_{p\text{IV}}$ (> 31), was plotted vs B at constant L, as in the foregoing.

3) Using McIlwain's spectrum variation, $E_0 = 306\,L^{-5.2}$, $J_{p\text{IV}}$ (>31) was converted to $J_{p\text{IV}}$ (40–110).

4) $J_{p\text{IV}}$ (40–110) was plotted vs B at constant L and then normalized to $J_{p\text{XV}}$ (40–110). When normalizing Explorer IV data to Explorer XV data, the correction for the change in atmospheric density was accomplished by shifting a constant value (0.015 gauss) along the B axis, as explained later.

5) In Fig. 1, J_p (40–110) isoflux contours were plotted in B, L coordinates. In this figure Explorer XV data is outlined with a heavy dashed line, and Explorer IV data is outlined in a heavy black line.

The other areas of the curve are extrapolations using the data from the other sources listed previously. As an example of the method, a sample calculation for J_p (40–110) at $L = 1.6$ follows:

1) The plot of $J_{p\text{XV}}$ (40–110) appears in Fig. 2.

2) The plot of $J_{p\text{IV}}$ (>31) appears in Fig. 3.

3) Using $E_0 = 306\,L^{-5.2}$, it follows that $E_0 = 26$ at $L = 1.6$, and

$$\frac{J_{p\text{IV}}\ (40\text{–}110)}{J_{p\text{IV}}\ (>31)} = \frac{KE_0e^{-40/26} - KE_0e^{-110/26}}{KE_0e^{-31/26}} \tag{16}$$

or

$$J_{p\text{IV}}\ (40\text{–}110) = \frac{e^{-40/26} - e^{-110/26}}{e^{-31/26}}\,J_{p\text{IV}}\ (>31)$$

Therefore,

$$J_{p\text{IV}}\ (40\text{–}110) = 0.66\,J_{p\text{IV}}\ (>31) \text{ at } L = 1.6$$

4) $J_{p\text{IV}}$ (40–110) is plotted with $J_{p\text{XV}}$ (40–110) in Fig. 2.

5) $J_{p\text{IV}}$ (40–110) was normalized to $J_{p\text{XV}}$ (40–110), as shown in Fig. 2.

In order to use Fig. 1, the B and L values encountered by a satellite can be found in Dudziak, Kleinecke, and Kostigen.[26]

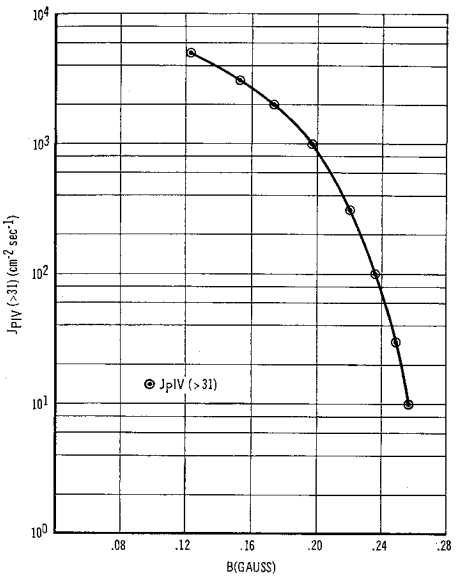

Fig. 3 Omnidirectional proton flux at $L = 1.6$ ($E > 31$ Mev).

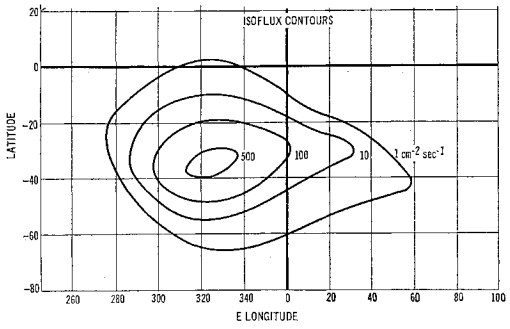

a) Protons ($40 < E < 110$ Mev), 400 km alt

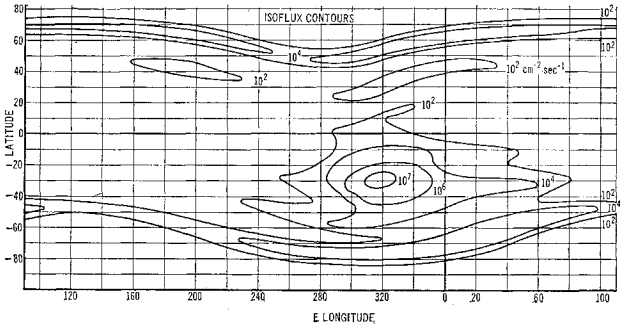

b) Electrons ($E > 0.5$ Mev), 400 km alt

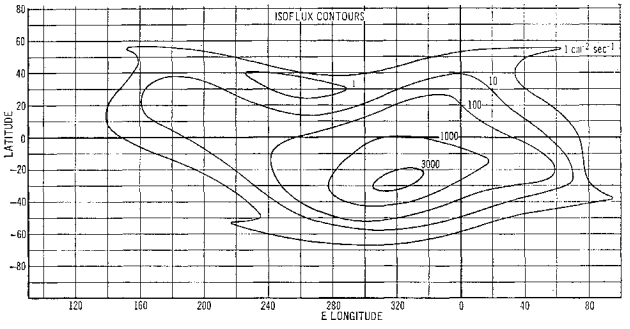

c) Protons ($40 < E < 100$ Mev), 1000 km alt

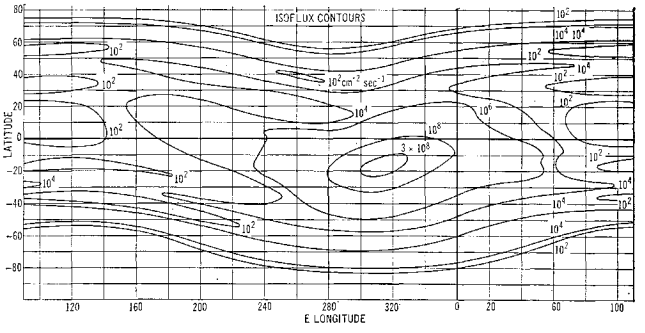

d) Electrons ($E > 0.5$ Mev), 1000 km alt

Fig. 4 Omnidirectional flux maps.

The flux maps can be converted to geographic coordinates, giving maps similar to those shown in Fig. 4.

The fluxes shown in Fig. 1 are normalized to January 1, 1963, and they will, in general, be different at other times. The effect will be to decrease the flux at low altitudes as the atmospheric density increases with the increase in solar activity near the peak of the solar cycle. An investigation[27] of the expected atmospheric density in 1968 indicates, for example, that the density now found at 400 km will, in 1968, be at about 470 km, and the density now at 1000 km will be at 1250 km. However, the relationship between flux and density is not simple; the change in altitude of constant density surfaces increases with altitude, whereas the change in altitude of constant flux surfaces decreases with altitude. Obviously, the relatively large atmospheric fluctuations at high altitudes (e.g., 1000 km) affect the flux profiles very little, because the magnitude of the density is so small. In addition, the state of solar activity in 1968 is a matter of speculation. Comparison of the data from 1958–1959, near solar maximum, to that from 1963, near solar minimum, shows that the flux of particles found at solar minimum at a position (B_1, L_1) will be found during solar maximum at the position ($B_1 - \Delta B$, L_1). The value of ΔB is approximately constant with L and equal to about 0.015 gauss at solar maximum for B_1 greater than 0.1 gauss. The assumption has been made that this effect will be the same over the next solar cycle, and that ΔB varies sinusoidally with a period of 11 years.

The proton data used here are based on Explorer XV and Air Force satellite measurements with extrapolations to other regions, as explained previously. McIlwain's data are good to within 30%,[16] whereas those of Freden and Paulikas are probably within a factor of two.[19] The fluxes in the high B regions are in the tail of the distribution, are no doubt less reliable, and are also subject to short-term variations. However, the fluxes used are "typical" values, and are adequate since they contribute only a small part of the total integrated flux. In general, when interpolations and extrapolations were made to produce the flux maps, the data indicating the highest fluxes were used when there was a choice to be made, and similarly the type of extrapolation which gave the highest fluxes in regions where no data were available was used. This technique was based on the philosophy that it is more desirable to overestimate the flux than to underestimate it.

A preliminary examination of recently published measurements[28] from Cosmos 3 and Cosmos 5, which were unavailable for inclusion in the data compilation, indicates good agreement with the material presented here. They include quite extensive coverage of the flux of protons having energies greater than 75 Mev.

3.3 Electrons from Artificial Sources

On July 9, 1962, a nuclear device designated "Starfish" was detonated at an altitude of about 400 km over Johnston Island, on an $L = 1.12$ geomagnetic field line. It injected some 10^{25} electrons with energies between 0.5 and 10 Mev into trapped orbits in the geomagnetic field. The peak flux at $L = 1.2$ to 1.3 on the equator was greater than 10^9 cm^{-2}-

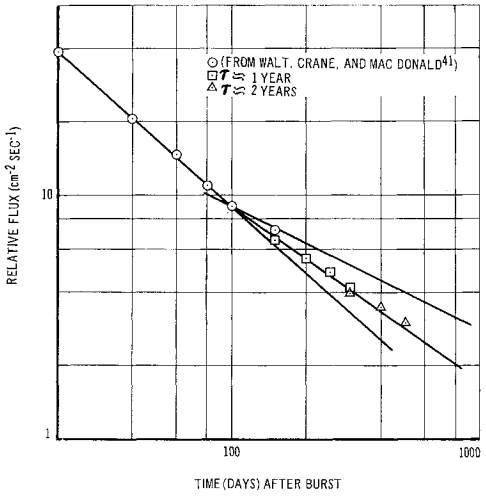

Fig. 5 Decay of "Starfish" artificial electrons.

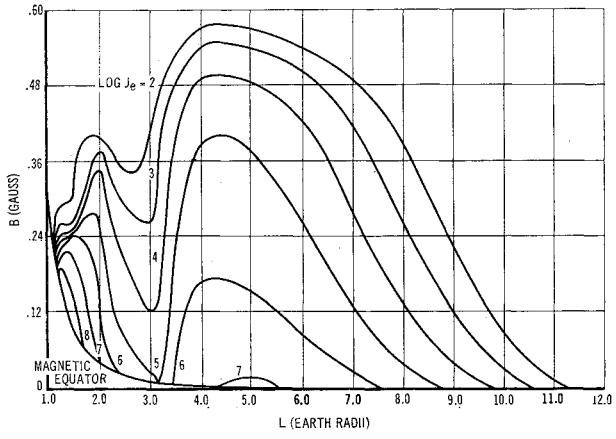

Fig. 6 Omnidirectional electron flux J_e ($E > 0.5$ Mev) in B, L coordinates.

sec^{-1}, and significant fluxes were found at altitudes as low as 100 km.

The immediate effect of the burst was to produce a large cloud of fission debris and intensive fluxes of gammas and neutrons. The gammas and neutrons were a brief hazard, since they are not trapped in the geomagnetic field. The neutrons decayed into protons and electrons, some of which were trapped in the geomagnetic field. However, the fluxes were quite low; the proton flux was negligibly small compared to the natural proton flux, and the electrons were barely detectable.[29] The cloud of fission fragments remained quite localized and diffused into the atmosphere in several days.[30] Immediately after the burst and at a decreasing rate for weeks afterward, this cloud produced fission decay electrons. Ordinarily, as demonstrated by the Argus series of high-altitude nuclear bursts,[3] the only fission electrons trapped in the geomagnetic field would have been those having pitch angles very near 90° on magnetic field lines in the immediate vicinity of the burst, resulting in a thin shell of artificial trapped electrons. However, the Starfish burst was so large that the energy density in the particle cloud was greater than the energy density in the magnetic field. This disrupted the magnetic field and allowed the fission debris to be distributed over a large range of L values, especially L values larger than 1.12. Electrons released at lower L values were quickly lost in the atmosphere.

Initially, these trapped fission electrons exhibited a distribution peaked at $L \approx 1.13$ and extended out to at least $L \approx 1.4$,[31] but after a few days the electrons on low L shells

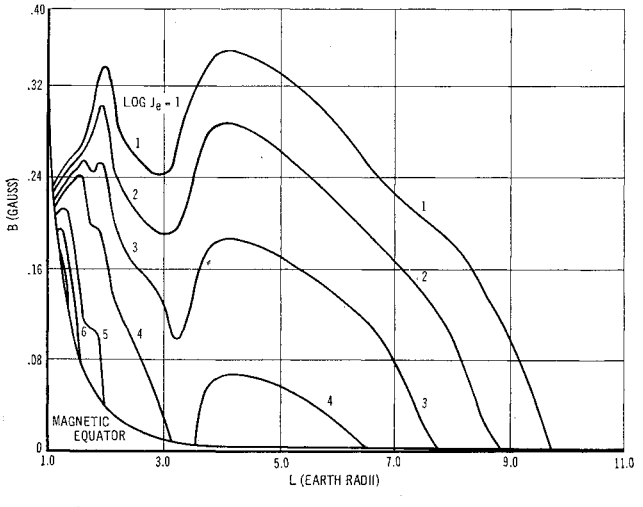

Fig. 7 Omnidirectional electron flux J_e ($E > 5.0$ Mev) in B, L coordinates.

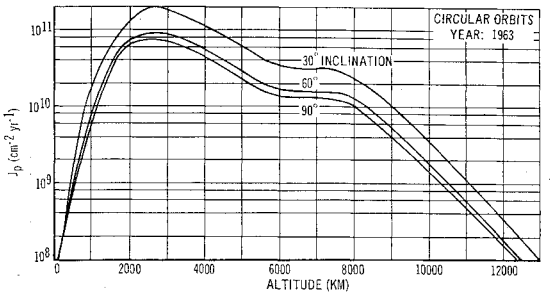

Fig. 8 Integrated proton flux vs altitude ($40 < E < 700$ Mev).

had been absorbed in the atmosphere, and the peak had shifted to $L \approx 1.2$.[32,33] There is no compelling evidence that Starfish fission electrons were trapped at values of L higher than 1.6.

The most complete artificial electron data available to date for this study were from Explorer XV[18] and Discoverer satellites 29 and 31.[34] The Explorer XV data for electrons with energy greater than 0.5 and 5 Mev were compared with Discoverer 29 and 31 data along with those from rockets,[21] Injun I,[35] Alouette,[36] Explorer XIV,[37] Explorer XII,[38] and polar orbiting Air Force satellites.[39] According to McIlwain,[16] the integral energy spectrum between 0.5 and 5 Mev is exponential within about 50%; this is supported by Starad measurements.[40] For electrons above 5 Mev, a fission spectrum is assumed which is consistent with Paulikas and Freden's[39] low high-energy fluxes.

The time decay of the artificial radiation is somewhat uncertain. The measurements of McIlwain on Explorer XV showed no measurable changes in fluxes at L values between 1.25 and 1.7 near the equator over a period of about three months at the end of 1962. An analysis of electron decay has been made by Walt, Crane, and MacDonald[41] and compared to data from Injuns I and III. In general, the results in the South Atlantic anomaly are in fair agreement. They indicate that, even at low altitudes, although the flux decreased significantly from the initial value to the January 1, 1963 value, the time τ for an e-fold decrease in flux was increasing. Also, they find that τ is not a function of B. The data from Walt, Crane, and MacDonald were replotted on log-log paper in Fig. 5. Estimates of the decay based on McIlwain's[18] and other data[42,43] yield values of τ of 1 and 2 years, respectively, if an exponential decay is assumed. These segments of exponential decay curves were replotted in Fig. 5 in their approximate regions of validity and normalized to Walt, Crane, and MacDonald's data. This technique of slope fitting can be done several ways, leading to various estimates of the time decay. It is concluded that the decay is probably of the form

$$J_e = J_{e0}\, t^{-\gamma} \tag{17}$$

with $\gamma = 0.9$ for $20 < t < 100$ days, and $\gamma = 0.7 \pm 0.2$ for $t > 100$ days. This is plotted in Fig. 5. Since the data pre-

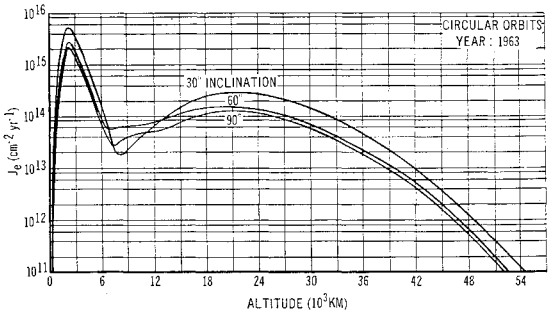

Fig. 9 Integrated electron flux vs altitude ($E > 0.5$ Mev).

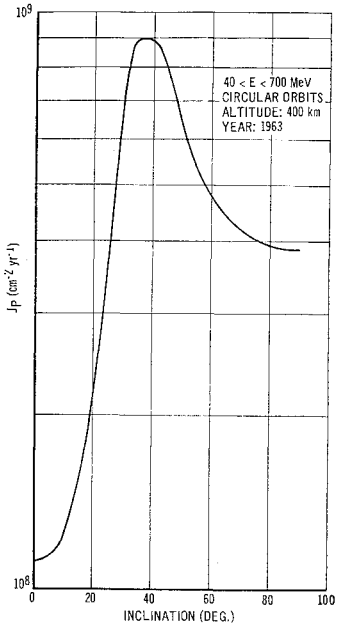

Fig. 10 Integrated proton flux vs inclination at 400-km alt.

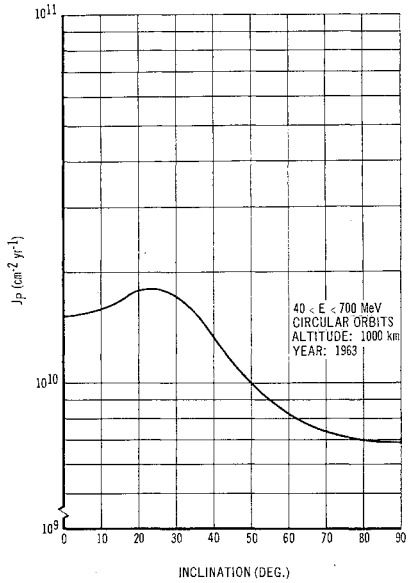

Fig. 12 Integrated proton flux vs inclination at 1000-km alt.

sented here are for $t \approx 175$ days, the equation

$$J_e = J_{e175}(t/175)^{-0.7\pm0.2} \tag{18}$$

can be used to calculate the flux at later times. In mid-1968 (day 2200), therefore,

$$J_{e2200} \approx \left(0.17 \begin{matrix} + 0.11 \\ - 0.07 \end{matrix}\right) J_{e175} \tag{19}$$

This does not take into account the changes in the atmosphere expected in 1968. These changes will result in a further reduction in the flux.

Measurements[44] made in late 1963 and early 1964 show a faster decay than is predicted by this model. Fluxes calculated using Eq. (19) will therefore be upper limits. If another large device were detonated at a low L value similar to Starfish, results could be expected to be similar to those described previously. The electrons released from bursts at high latitudes, and therefore high L values, are rapidly depleted by magnetic field fluctuations and atmospheric loss.[18]

Russian nuclear devices were detonated in late 1962 at high altitudes and higher latitudes than Starfish. Measurements have been made of the time decay of these bursts and indicate exponential-like decays with time constants of the order of days.[45] The peak fluxes, as measured by McIlwain with Explorer XV and by Air Force satellites,[46] were considerably smaller than the Starfish peak, consistent with a less efficient injection mechanism at high L values, or a smaller yield. Independent measurements[47] of the decay rates of these Soviet-produced electrons indicate a power-law decay in agreement with the assumptions made here.

3.4 Natural Electrons

For L less than 2 there are very little data on the natural, or pre-Starfish, electron flux. Data taken since Starfish include both natural and artificial electrons and are in themselves of very limited usefulness for determining the natural electron flux. However, comparison with early measurements[21] indicates that the variation of the natural electron flux with

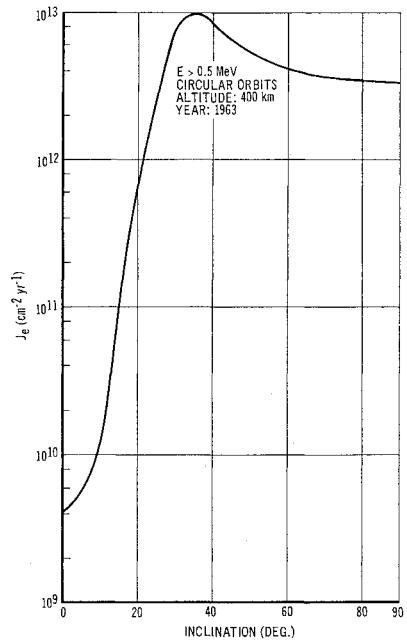

Fig. 11 Integrated electron flux vs inclination at 400-km alt.

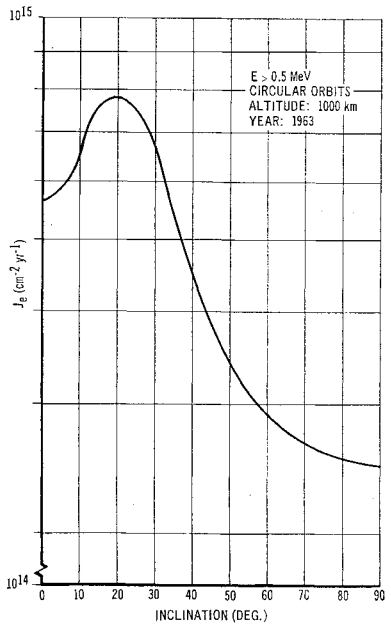

Fig. 13 Integrated electron flux vs inclination at 1000-km alt.

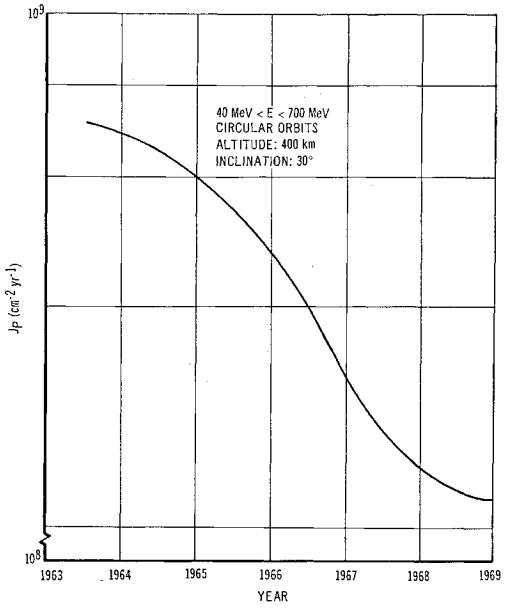

Fig. 14 Integrated proton flux variation over the solar cycle at 400-km alt.

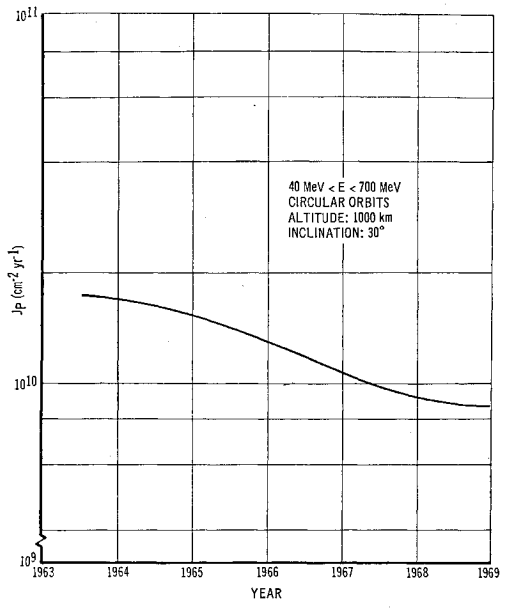

Fig. 16 Integrated proton flux variation over the solar cycle at 1000-km alt.

altitude is not greatly different from the variation of the total electron flux as measured by Explorer XV.[18] The variation of the natural electron flux with position is sufficiently similar to that of the total flux that the total flux distribution curve can be used for the natural flux distribution when they are properly normalized. A safe upper limit for the natural electron flux can be found by assuming that the electrons in this inner zone region have an altitude-independent integral spectrum of the form[21,31]

$$\begin{aligned} J_e\,(>E) &= K_1\,E^{-0.5} \qquad 30 < E < 200 \text{ kev} \\ J_e\,(>E) &= K_2 E^{-4} \qquad 0.2 < E < 5 \text{ Mev} \end{aligned} \tag{20}$$

and that the natural electron flux with energy greater than 180 kev is numerically equal to the total flux greater than 0.5 Mev as of January 1, 1963.

The scarcity of good data and the existence of sporadic, short-term variations prohibit estimates of electron fluxes to better than an order of magnitude for L values greater than 2. It therefore may be assumed that, for $2 < L < 10$, at an altitude of 1000 km, the electron flux for $E > 40$ kev is approximately 10^6 cm^{-2}-sec^{-1}.[48] The electron spectrum for energies greater than 0.5 Mev was measured by Explorer XV for values of L up to 4, and by Explorer XIV[37] at high altitudes near the equator. This spectrum is relatively hard at high energies but is supported by Explorer XII measurements.[38,49]

A procedure was followed for the electrons similar to that used to determine the proton flux distributions, again based on Explorer XV data. However, no additional set of data comparable in quantity to the Explorer IV data for protons was available, so each set of data used for the electron extrapolation was individually corrected to the proper energy range, making sure that the spectrum did vary regularly with L and B. The resulting flux distributions are shown in Fig. 6 for electrons having energies greater than 0.5 Mev and in Fig. 7 for electrons having energies greater than 5.0 Mev.

4. Conclusions

As stated previously, the purpose of this report is to present the available geomagnetically trapped radiation data in a

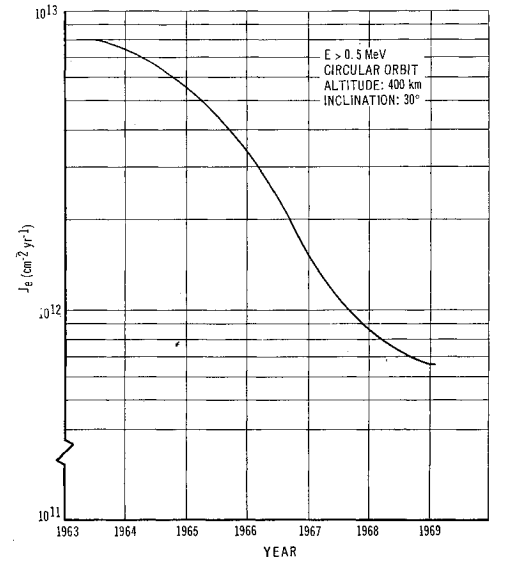

Fig. 15 Integrated electron flux variation over the solar cycle at 400-km alt.

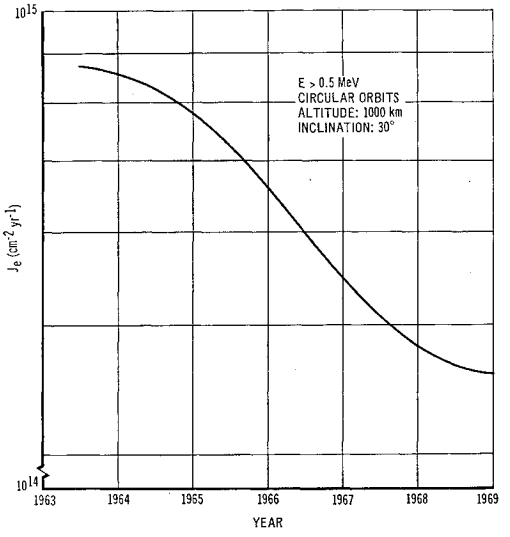

Fig. 17 Integrated electron flux variation over the solar cycle at 1000-km alt.

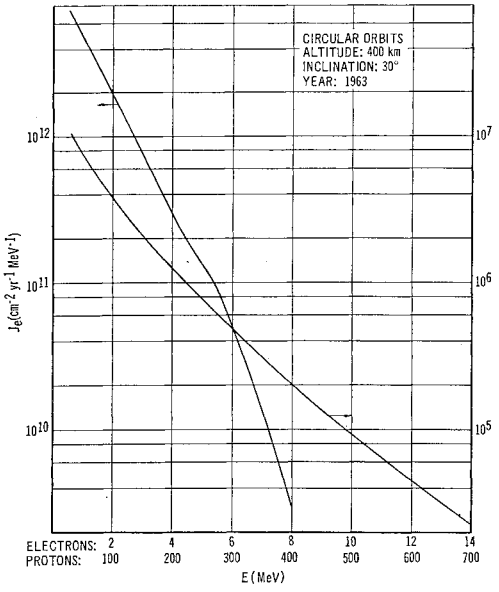

Fig. 18 Proton and electron time-integrated differential energy spectra (400 km, 30°).

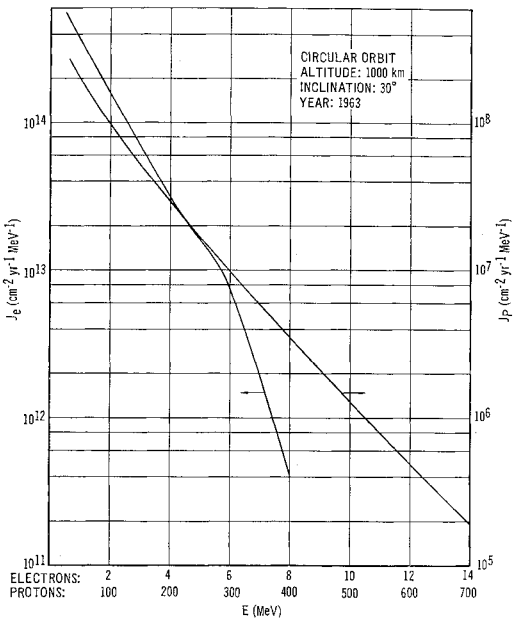

Fig. 20 Proton and electron time-integrated differential energy spectra (1000 km, 30°).

form that is useful for designing radiation shields and for calculating doses.

A computer program has been developed which calculates the exposure of satellites to trapped particles and solar cosmic-ray protons. It either traces the satellite orbit or computes the amount of time spent by the satellite in each of many small regions of space. The entire volume that the satellite eventually covers is divided up into these small increments in a manner similar to that described by Sowle and Lowen.[50]

In high-inclination orbits, a satellite may be exposed to solar cosmic radiation. The radiation consists of protons, alphas, and heavy nuclei.[51] The intensities of solar cosmic-ray events vary considerably; the total flux of high-energy protons produced by all small events probably amounts to less than 20% of the flux from large (e.g., November 12, 1960) events. We have chosen the November 12, 1960 event as a model because it was the largest studied, excluding the poorly observed July 14, 1959 event; its spectrum is similar to many other events and includes high-energy (Gev) particles; and it is the event for which we have the most complete data.[52] The time-integrated differential energy spectrum for the November 1960 event is

$$J_p(E) = 1.77 \times 10^{13} E^{-3} \text{ cm}^{-2}\text{-Mev}^{-1} \qquad 30 < E < 80 \text{ Mev}$$

$$J_p(E) = 9.62 \times 10^{16} E^{-5} \text{ cm}^{-2}\text{-Mev}^{-1} \qquad 80 < E < 440 \text{ Mev} \quad (21)$$

$$J_p(E) = 6.63 \times 10^{18} E^{-5.4} \text{ cm}^{-2}\text{-Mev}^{-1} \qquad 440 < E < 6600 \text{ Mev}$$

An earth-orbiting satellite will be partially shielded by the geomagnetic field. The geomagnetic field alters the trajectories of incoming charged particles in such a way that all particles with less than a certain "cutoff" energy do not penetrate the field. The vertical cutoff energy, the minimum

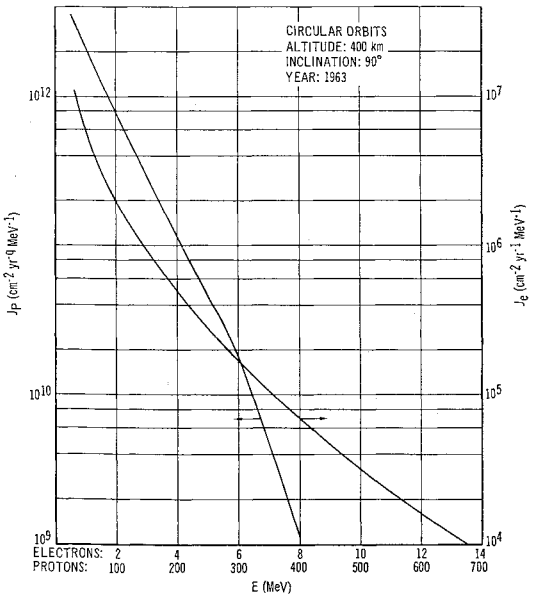

Fig. 19 Proton and electron time-integrated differential energy spectra (400 km, 90°).

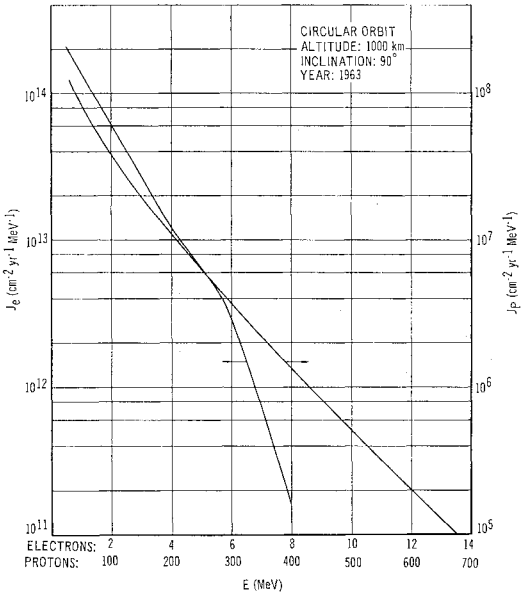

Fig. 21 Proton and electron time-integrated differential energy spectra (1000 km, 90°).

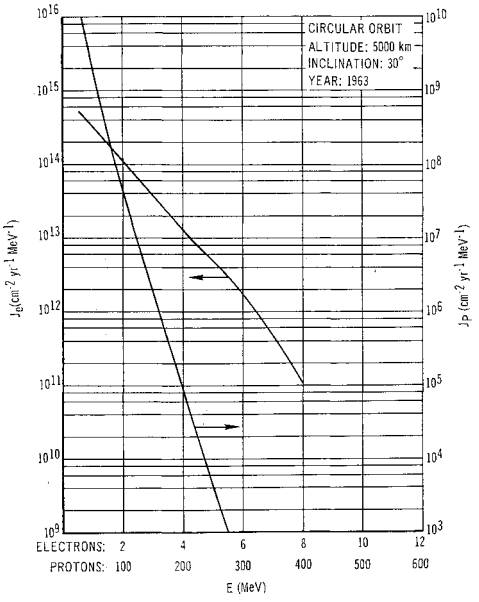

Fig. 22 Proton and electron time-integrated differential energy spectra (5000 km, 30°).

energy that charged particles must have to penetrate the field to the top of the atmosphere from the zenith, shows a dependence on L that is nearly independent of position.[53] According to calculations based on measurements by Explorer VII,[54] the cutoff energy could be expressed as

$$E_c = 2.5 \times 10^5 e^{-L/.35} \text{ Mev} \qquad (22)$$

during the November 12, 1960 event. Each time L is computed by the program, the cutoff energy is calculated using this equation and fluxes at higher energies accumulated using the spectrum given previously. In this way, the energy spectrum that would be encountered by a satellite during an identical event is determined.

The conclusions of this report consist of the results of running the computer program: the fluxes and energy spectra of protons and electrons for satellite orbits. Although many computer runs have been made, it is unlikely that any of the orbits included would exactly coincide with the requirements of the reader. Therefore, it has been decided to include only graphical samples of the circular orbit calculations. All used the approximate method of time integration,[50] and all are for a duration of one year. Elliptic orbits and shorter durations have been run but not enough to provide the comparisons that can be made using the circular, one-year runs.

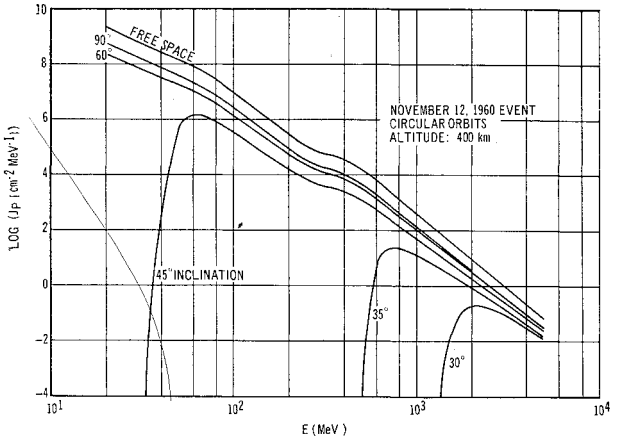

Fig. 23 Time-integrated solar cosmic-ray proton differential energy spectra vs inclination.

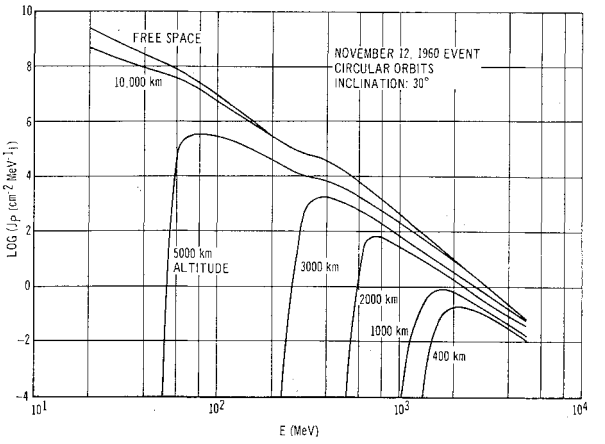

Fig. 24 Time-integrated solar cosmic-ray proton differential energy spectra vs altitude.

Figures 8 and 9 show the total proton and electron fluxes as a function of altitude for three different inclinations. Figures 10–13 show the total flux variation with orbital inclination at two different altitudes. The peak due to the large flux in the South Atlantic magnetic anomaly at about 35° latitude is easily seen, especially at the lower altitude. Figures 14–17 illustrate the flux dependence on the atmospheric changes over the solar cycle. It was assumed that solar minimum was 1963.5, and the next maximum will be 1969.0. As the cycle progresses to another minimum in 1974, the proton flux will increase again to about the 1963.5 level. The electron flux at L values less than about 2, however, will not increase, assuming no more high-altitude nuclear tests, since at these high energies it is composed largely of artificially injected fission electrons. Also superimposed on the decay shown here, which applies to all trapped particles, is the measured decay of the artificial electrons discussed previously. Finally, Figs. 18–22 show plots of sample differential energy spectra, and Figs. 23 and 24 show the solar cosmic-ray differential energy spectra for various inclinations and altitudes.

References

[1] Singer, S. F., "A new model of magnetic storms and aurorae," Trans. Am. Geophys. Union **38,** 175–190 (1957).

[2] Van Allen, J. A., Ludwig, G. H., Ray, E. C., and McIllwain, C. E., "Observations of high intensity radiation by satellites 1958 Alpha and Gamma," Jet Propulsion **28,** 588–592 (1958).

[3] Christofilos, N. C., "The Argus experiment," J. Geophys. Res. **64,** 869–876 (1959).

[4] Hess, W. N., "The effects of high-altitude explosions," *Space Physics,* edited by D. P. LeGalley and A. Rosen (John Wiley and Sons, Inc., New York, 1964), pp. 573–610.

[5] Alfvén, H., *Cosmical Electrodynamics* (Clarendon Press, Oxford, England, 1950).

[6] Northrop, T. G. and Teller, E., "Stability of the adiabatic motion of charged particles in the earth's field," Phys. Rev. **117,** 215–225 (1960).

[7] Northrop, T. G., "Adiabatic charged-particle motion," Rev. Geophys. **1,** 283–304 (1963).

[8] McIlwain, C. E., "Coordinates for mapping the distribution of magnetically trapped particles," J. Geophys. Res. **66,** 3681–3692 (1961).

[9] Jensen, D. C. and Cain, J. C., "An interim geomagnetic field," American Geophysical Union Meeting, Paper P 1 (April 1962).

[10] Van Allen, J. A. and Frank, L. A., "Radiation around the earth to a radial distance of 107,400 km.," Nature **183,** 430–434 (1959).

[11] Kellogg, P. J., "Possible explanation of the radiation observed by Van Allen at high altitudes in satellites," Nuovo Cimento **11,** 48–66 (1959).

[12] Singer, S. F., "Trapped albedo theory of the radiation belts," Phys. Rev. Letters **1,** 181–183 (1958).

[13] Lenchek, A. M. and Singer, S. F., "The albedo neutron

theory of geomagnetically trapped protons," Planetary Space Sci. **11**, 1151–1208 (1963).

[14] Hess, W. N., Canfield, E. H., and Lingenfelter, R. E., "Cosmic ray neutron demography," J. Geophys. Res. **66**, 665–678 (1961).

[15] O'Brien, B. J., "The trapped-radiation zones," *Space Physics*, edited by D. P. LeGalley and A. Rosen (John Wiley and Sons, Inc., New York, 1964), pp. 503–572.

[16] McIlwain, C. E., personal communication, Univ. of California, San Diego, Calif. (1963).

[17] McIlwain, C. E. and Pizzella, G., "On the energy spectrum of protons trapped in the earth's inner Van Allen zone," J. Geophys. Res. **68**, 1811–1824 (1963).

[18] McIlwain, C. E., "The radiation belts, natural and artificial," Science **142**, 355–361 (1963).

[19] Freden, S. C. and Paulikas, G. A., "Trapped protons at low altitudes in the South Atlantic magnetic anomaly," J. Geophys. Res. **69**, 1259–1269 (1964).

[20] Pizzella, G., McIlwain, C. E., and Van Allen, J. A., "Time variations of intensity in the earth's inner radiation zone, October 1959 through December 1960," J. Geophys. Res. **67**, 1235–1254 (1962).

[21] Holly, F. E., Allen, L., Jr., and Johnson, R. G., "Radiation measurements to 1500 kilometers altitude at equatorial latitudes," J. Geophys. Res. **66**, 1627–1640 (1961).

[22] Seward, F. D. and Kornblum, H. N., Jr., "Near-earth charged-particle backgrounds measured with polar orbiting satellites," Univ. of California Lawrence Radiation Lab. Paper UCRL-6693, Livermore, Calif. (1963).

[23] Ginzburg, V. L., Kurnosova, L. V., Logachev, V. I., Rozarenov, L. A., Sirotkin, I. A., and Fradkin, M. I., "Investigation of charged particle intensity during the flights of the second and third space-ships," Planetary Space Sci. **9**, 845–854 (1962).

[24] Vernov, S. I., Savenko, I. A., Shavrin, P. I., and Pisarenko, N. F., "Detection of an inner radiation belt at the altitude of 320 km in the region of the South Atlantic magnetic anomaly," Planetary Space Sci. **9**, 861–865 (1962).

[25] Fillius, R. W. and McIlwain, C. E., "Anomalous energy spectrum of protons in the earth's radiation belt," Phys. Rev. Letters **12**, 609–612 (1964).

[26] Dudziak, W. F., Kleinecke, D. D., and Kostigen, T. J., "Graphic displays of geomagnetic geometry," RM63TMP-2, DASA 1372, TEMPO, General Electric Co., Santa Barbara, Calif. (1963).

[27] Wasko, P. E. and Michaux, C. M., "Earth's aerospace thermodynamic properties from 100 to 100,000 km altitude above Cape Kennedy expected for the 1962–1973 period," Douglas Paper 1934, Douglas Aircraft Co., Inc., Santa Monica, Calif. (1964).

[28] Temny, V. V., "An atlas of corpuscular intensity levels, registered with the aid of the Cosmos-3 and Cosmos-5 satellites," *Space Research V*, edited by D. G. King-Hele, P. Muller, and G. Righini (North-Holland Publishing Co., Amsterdam, the Netherlands, 1965), pp. 489–497.

[29] Durney, A. C., Elliot, H., Hynds, R. V., and Quenby, J. J., "The artificial radiation belt produced by the 'Starfish' nuclear explosion," Imperial College of Science and Technology Paper, London (June 1963).

[30] Pieper, G. F., "A second radiation belt from the July 9, 1962, nuclear detonation," J. Geophys. Res. **68**, 651–656 (1963).

[31] O'Brien, B. J., Laughlin, C. D., and Van Allen, J. A., "Geomagnetically trapped radiation produced by a high altitude nuclear explosion on July 9, 1962," Nature **195**, 939–943 (1962).

[32] Hess, W. N., "The artificial radiation belt made on July 9, 1962," J. Geophys. Res. **68**, 667–684 (1963).

[33] Van Allen, J. A., Frank, L. A., and O'Brien, B. J., "Satellite observations of the artificial radiation belt of July 1962," J. Geophys. Res. **68**, 619–628 (1963).

[34] Mann, L. G., Bloom, S. D., and West, H. I., Jr., "The electron spectrum from 90 to 1200 keV observed on Discoverer satellites 29 and 31," *Space Research III*, edited by W. Priester (North-Holland Publishing Co., Amsterdam, 1963), pp. 447–462.

[35] O'Brien, B. J., "Review of studies of trapped radiation with satellite-borne apparatus," Space Sci. Rev. **1**, 415–484 (1963).

[36] McDiarmid, I. B., Burrows, J. R., Budzinski, E. E., and Rose, D. C., "Satellite measurements in the 'Starfish' artificial radiation zone," Div. of Pure Physics, Natural Research Council, Ottawa, Canada (1963).

[37] Frank, L. A., Van Allen, J. A., Whelpley, W. A., and Craven, J. D., "Absolute intensities of geomagnetically trapped particles with Explorer 14," J. Geophys. Res. **68**, 1573–1580 (1963).

[38] O'Brien, B. J., Van Allen, J. A., Laughlin, C. D., and Frank, L. A., "Absolute electron intensities in the heart of the earth's outer radiation zone," J. Geophys. Res. **67**, 397–403 (1962).

[39] Paulikas, G. A. and Freden, S. C., "Precipitation of energetic electrons into the atmosphere," J. Geophys. Res. **69**, 1239–1249 (1964).

[40] West, H. I., Jr., Mann, L. G., and Bloom, S. D., "Some electron spectra in the radiation belts in the fall of 1962," Univ. of California Lawrence Radiation Lab. Rept. UCRL-7659 (1964).

[41] Walt, M., Crane, G. E., and MacDonald, W. M., "Analysis of atmospheric scattering loss rates for geomagnetically trapped electrons," American Geophysical Union Meeting, Paper P 50 (April 1963).

[42] McIlwain, C. E., "Trapped radiation intensities in November, 1962," Operation Fishbowl Review Symposium (I), DASA, Chicago, Ill. (November 1963).

[43] Van Allen, J. A., "SUI analyses and model of the artificial belts," Operation Fishbowl Review Symposium (I), DASA, Chicago, Ill. (November 1963).

[44] Bostrom, C. O. and Williams, D. J., "Time decay of the artificial radiation belt," J. Geophys. Res. **70**, 240–242 (1965).

[45] Giacconi, R., Paolini, F. R., and Katz, L., "Measurement of trapped particles injected by nuclear detonations," American Geophysical Union Meeting, Paper P 46 (April 1963).

[46] White, R. S., "Measurements of Soviet electrons from Soviet tests," Goddard Space Flight Center Trapped Radiation Symposium, Greenbelt, Md. (April 1963).

[47] Burrows, J. R. and McDiarmid, I. B., "A study of beta-decay electrons injected into the geomagnetic field in October 1962," Div. of Pure Physics, National Research Council, Ottawa, Canada (1964).

[48] O'Brien, B. J., "Lifetimes of outer-zone electrons and their precipitation into the atmosphere," J. Geophys. Res. **67**, 3687–3706 (1962).

[49] Farley, T. A., "The growth of our knowledge of the earth's outer radiation belt," Rev. Geophys. **1**, 3–34 (1963).

[50] Sowle, D. H. and Lowen, R. W., "Calculation of average radiation fluxes on satellites," J. Spacecraft Rockets **2**, 153–159 (1965).

[51] Biswas, S., Fichtel, C. E., and Guss, D. E., "Study of the hydrogen, helium, and heavy nuclei in the November 12, 1960 solar cosmic-ray event," Phys. Rev. **128**, 2756–2771 (1962).

[52] Masley, A. J. and Goedeke, A. D., "Complete dose analysis of the November 12, 1960, solar cosmic ray event," *Life Sciences and Space Research*, edited by R. B. Livingston, A. A. Imshenetsky, and G. A. Derbyshire (North-Holland Publishing Co., Amsterdam, 1963), pp. 95–109.

[53] Lin, W. C., Vankatesan, D., and Van Allen, J. A., "Latitude survey of cosmic ray intensity by Explorer 7, October 1959 to February 1961," J. Geophys. Res. **68**, 4885–4896 (1963).

[54] Lin, W. C. and Van Allen, J. A., "Observation of solar cosmic rays from October 13, 1959, to February 17, 1961 with Explorer VII," State Univ. of Iowa Research Rept. SUI 63-15 (1963).